# PHILOSOPHICAL TRANSACTIONS A

royalsocietypublishing.org/journal/rsta

#### Research



**Cite this article:** Milne ZB, Hasz K, McClimon JB, Castro J, Carpick RW. 2022 A modified multibond model for nanoscale static friction. *Phil. Trans. R. Soc. A* **380**: 20210342. https://doi.org/10.1098/rsta.2021.0342

Received: 30 December 2021 Accepted: 28 February 2022

One contribution of 12 to a theme issue 'Nanocracks in nature and industry'.

#### **Subject Areas:**

mechanical engineering, nanotechnology

#### **Keywords:**

nanoscale friction, stick slip, atomic force microscopy, surface science, tribology, statistical mechanics, nanotribology, Prandtl-Tomlinson model

#### **Author for correspondence:**

Robert W. Carpick

e-mail: carpick@seas.upenn.edu

<sup>†</sup>Present address: Department of Physics, Carthage College, University of Colorado.

Electronic supplementary material is available online at https://doi.org/10.6084/m9.figshare. c.6026343.

# THE ROYAL SOCIETY

# A modified multibond model for nanoscale static friction

Zachary B. Milne<sup>1</sup>, Kathryn Hasz<sup>2,†</sup>,

J. B. McClimon<sup>1</sup>, Juan Castro<sup>3</sup> and Robert W. Carpick<sup>1</sup>

<sup>1</sup>Department of Mechanical Engineering and Applied Mechanics, <sup>2</sup>Department of Materials Science and Engineering, and <sup>3</sup>Department of Physics and Astronomy, University of Pennsylvania, Philadelphia, PA, USA

ZBM, 0000-0003-2000-5901; KH, 0000-0003-3089-2882;
JBM, 0000-0002-2163-7495; RWC, 0000-0002-3235-3156

Several key features of nanoscale friction phenomena observed in experiments, including the stick-slip to smooth sliding transition and the velocity and temperature dependence of friction, are often described by reduced-order models. The most notable of these are the thermal Prandtl-Tomlinson model and the multibond model. Here we present a modified multibond (mMB) model whereby a physically-based criterion—a critical bond stretch length—is used to describe interfacial bond breaking. The model explicitly incorporates damping in both the cantilever and the contacting materials. Comparison to the Fokker-Planck formalism supports the results of this new model, confirming its ability to capture the relevant physics. Furthermore, the mMB model replicates the near-logarithmic trend of increasing friction with lateral scanning speed seen in many experiments. The model can also be used to probe both correlated and uncorrelated stick slip. Through greater understanding of the effects of damping and noise in the system and the ability to more accurately simulate a system with multiple interaction sites, this model extends the range of frictional systems and phenomena that can be investigated.

This article is part of the theme issue 'Nanocracks in nature and industry'.

#### 1. Introduction

Nanoscale friction has been studied experimentally, using approaches like the atomic force microscope (AFM) [1,2] and the surface force apparatus (SFA) [3], and has enjoyed theoretical exploration for far

sliding.

Downloaded from https://royalsocietypublishing.org/ on 09 August 2022

longer [4,5]. While the simple Coulomb picture of macroscale friction involves no speed or temperature dependence of friction, both factors can influence nanoscale friction. Several researchers have observed and documented an approximately logarithmic increase of kinetic friction with increasing scanning speed over several decades of speed [6-18]. Some of those studies and others report a decrease in friction with increasing temperature, at least over certain temperature ranges, leading to very low friction at elevated temperatures; this has been dubbed 'thermolubricity' [9-11,18-20]. These speed and temperature effects have been postulated to originate in the ability of thermal fluctuations to assist in overcoming static friction by providing thermal energy to either cleave interfacial bonds or overcome other local energy barriers to

Several models have been employed to explain the temperature and speed-dependent behaviour seen in these experiments and simulations. The thermal Prandtl-Tomlinson (PTT) model is the most widely used model [4,5,21]. When applied to a tip-sample contact in AFM, the tip is considered as a point mass attached to a fixed point by a spring, where the spring represents the lateral compliance in the system from the cantilever, the tip-sample contact, and the tip structure [22,23]. The point mass also interacts with a corrugated countersurface representing the (assumed) periodic energy landscape of the sample. That countersurface is being pulled at a constant speed. At zero temperature, as the puller moves at a constant speed, energy builds up in the spring and the tip-sample interaction (causing the 'stick' in 'stick-slip') until the system no longer resides in a potential minimum, forcing it to slip, often coming to rest at the next local minimum. Thermal energy in the form of vibrations assists this transition. The analytical form of the model predicts the logarithmic increase of friction with speed and decrease of friction with temperature. It has been used to fit experimental and simulation data across a range of sliding speeds and agrees well with many experimental results (e.g. [6,8,12-18]).

Another body of research, originating with Filippov with contributions by, among others, Schirmeisen, Barel and Urbakh, presents a different model for static friction, one that uses numeric simulations [7,9-11,19]. In their model, known as the multibond (MB) model, multiple local interactions or 'bonds' exist across the tip-sample interface. These local interactions could come from covalent bonds, polar bonds, localized van der Waals interactions or other interactions at localized regions within the contact due, for example, to nanoscale or even atomic roughness; the specific physical source is not stipulated. Each of those bonded interactions has a statistical chance of breaking and then a statistical chance for re-forming at any timestep. The MB model produces results that qualitatively agree with several experimental results for a variety of tip-sample pairs. Results show a similar logarithmic dependence of friction on speed as the PTT model [9–11,19], and a non-monotonic change of friction with temperature, with friction first increasing at low temperatures until a critical temperature, after which it decreases [9-11,19].

In the present paper, the physical origins of the modelling techniques used in the PTT and MB frameworks are discussed, and some of their limitations and assumptions are considered. A new theoretical model that addresses these limitations and assumptions, the modified multibond (mMB) model, is introduced and explored using numeric simulations. This new model, like the PTT and MB models, can replicate the logarithmic speed dependence often observed in AFM experiments, but its foundations are more general and more rigorous. One outcome of this generality and rigor is a more flexible model which has the ability to not only describe how friction changes with speed, damping, noise level and temperature, but also provides a practical algorithm to explore interesting testable predictions, notably, a potential downturn or levelling of friction at higher speeds. Such a levelling was initially proposed by Reimann and Evstigneev for the case of a PTT-like model with a single bond and periodic potential [24], but it likely occurs at speeds higher than those regularly accessed with AFM.

A unique aspect of the mMB model introduced here is to enforce a critical stretch length,  $X_c$ , which gives a hard cutoff for the bond stretch length at which the bond breaks. Though a critical stretch length is implied by the PTT model, the MB model does not use one. The mMB model benefits from a recent model that used a critical stretch length to describe nanoscale wear behaviour; results of that model matched well with experiments [25]. The mMB model also incorporates the effects of damping within the system, which is ignored in the PTT derivations used in refs [7,8,12–14,26,27]. Notably, in addition to the new insights contained in the mMB model, a new theoretical foundation for nanoscale friction simulations is explored in this work. As discussed further below, instead of a reliance on the traditionally used Master Equation Method (MEM) to calculate the probability that an interaction has not yet broken, as is done in applying the PTT model, ideas from the fundamental statistical mechanics in the Fokker–Plank (FP) equation are used to calculate this probability. Numerical solutions using the mMB model agree with those found with the FP equation, lending credibility to the mMB model.

### Existing reduced-order models of nanoscale friction

Both the PTT and MB models aim to describe the role of thermal noise on friction. Though they approach this problem in unique ways, their conceptual explanations of the speed dependence of friction that is often observed in nanoscale friction experiments are similar. Below, we discuss limitations in the microscopic description of the interactions controlling friction and methods to introduce improvements.

The essential elements of a reduced order model to describe the interactions controlling friction in AFM experiments are depicted in figure 1. This system comprises: a mass m; two springs—one each for the cantilever,  $k_{\rm cantilever}$ , and for the tip/sample bond (interaction) at the contact,  $k_{\rm bond}$ ; and two dampers—one each for the cantilever  $\eta_{\rm cantilever}$  and the bond  $\eta_{\rm bond}$ . Note that the experimentally observable effects of compliance of the tip structure and the contact compliance can be accounted for through  $k_{\rm cantilever}$ . In the PTT model presented in [14,15,26,27], the bond potential is periodic (often sinusoidal) rather than harmonic (spring) as in figure 1. The general analytical approach in the present paper applies to any bond potential, but a harmonic potential is used here to be consistent with the MB model [9–11,19]. In the MB model, there are arbitrarily many copies n of the spring and damper components labelled 'bond' in figure 1, each with a unique history-dependent x. The simplest case of n=1 will be the focus of discussion here, although the approach presented here, like the MB model, can be applied to an arbitrary number of bonds.

In the model system, the mass with position X vibrates from thermal and mechanical noise while being translated by a puller with time-dependent position x = vt attached to it via a spring with compliance  $k_{\text{bond}}$  and a damper with damping constant  $\eta_{\text{bond}}$ . Due to the vibrations, the bond will be broken with the help of large-amplitude, low-probability vibrations earlier than the pulling alone would break it. The faster the straining, the less likely one such vibration will occur in a given sliding distance and thus the cantilever spring will on average stretch farther before breaking than at slower speeds. After breaking the bond, the cantilever spring relaxes and thus a slip occurs.

Framing this explanation in the context of the AFM experiments used to test this prediction, the puller is analogous to moving the sample relative to the fixed cantilever base, and the bond (or multiple bonds, if more than one bond were to be modelled) is analogous to the attraction across the interface between the tip and sample. Since higher speeds lead to higher cantilever stretch (or in the case of AFM, torsion), the measured kinetic friction force is, barring other effects, greater at high speeds than at slower speeds. As mentioned above, the MB model predicts a logarithmic dependence of friction on pulling speed, in agreement with many experiments [7,8,12–18]. It predicts a non-monotonic dependence of friction on temperature, with a maximum value of friction at an intermediate temperature, also in agreement with experiments [7,8,12–18].

#### 3. The PTT model

The PTT model is perhaps the most widely used model for interpreting nanoscale friction results that show a dependence of friction on sliding speed. Several AFM studies exploring the speed dependence of friction have used PTT to interpret and explain experimental results

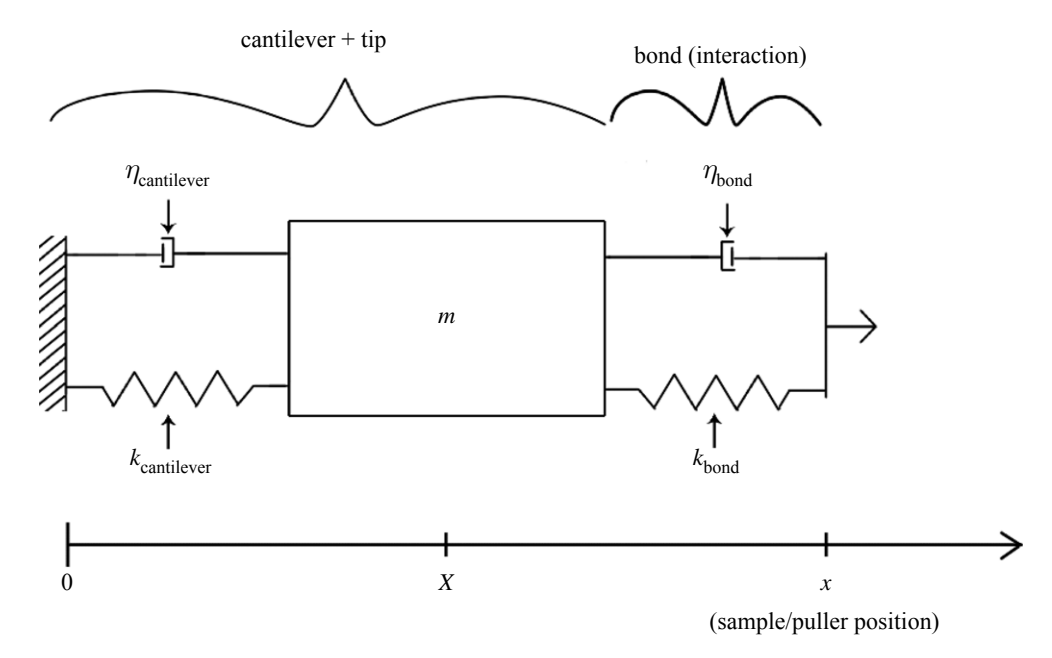


**Figure 1.** The dynamic friction system. The tip-sample bond is modelled as a collection of copies n of a spring (with elastic constant  $k_{\text{bond}}$ ) and a damper (with damping constant  $\eta_{\text{bond}}$ ), all connected between the tip mass and the sample. Modelled this way, the sample can be n bonds or local interactions with the tip. Only one such bond is shown in the example above. The cantilever is modelled as a spring (with elastic constant  $k_{\text{cantilever}}$ ) and a damper (with damping constant  $\eta_{\text{cantilever}}$ ).

[7,8,12–18]. The PTT model abstracts the behaviour of many interfacial bonds (*n* copies) into a single interaction: the interfacial potential. In the PTT model, the mass always resides somewhere along the interfacial potential, so the bond is always present, even after slip. This is one of the characteristics of the PTT model that distinguishes it from the MB model where the interaction can be broken and remain non-interacting for some time. Furthermore, the potential is rigid, i.e. unchanging with time or other conditions; it only depends on the single spatial coordinate of the tip. The analytical approach taken by several of the original proponents of the model [7,8,12–18] is to use the Master Equation Method (MEM) as a differential equation describing the probability that the bond has not slipped to the next energy minimum.

While the MEM approach can be effective and is responsible for the very useful transcendental equation for nanoscale friction, it does have some important limitations. These will carefully be explained here.

The derivation of  $F_f = F_f(v)$  in the PTT model begins with the Master Equation for the probability that a bond has not broken, P. Following the conventions of refs [26,27], the Master Equation is, generally:

$$\frac{\mathrm{d}P(vt)}{\mathrm{d}t} = -\gamma(vt)P(vt),\tag{3.1}$$

where v is the stretching speed of the puller (the speed of the sample in figure 1), t is the time where t=0 corresponds to the beginning of the sticking portion, and  $\gamma$  is the rate of breaking (equivalent to a *reaction rate* in kinetics). This rate is taken as *Kramer's rate*, which is  $\gamma = f_0 \exp(-\Delta E(vt)/k_bT)$ . The energy barrier to sliding is  $\Delta E(vt)$  and the attempt frequency is  $f_0$ . The position of the puller is given by vt.

Since the MEM relies on a probability equation, it should describe the behaviour of a large sample with initial population  $N_0$  and  $P = N/N_0$ . Thus

$$\frac{\mathrm{d}N(vt)}{\mathrm{d}t} = -\gamma(vt)N(vt),\tag{3.2}$$

where N is the independent random variable representing the number of bonds in the statistical sample that still have not slipped or broken.

The first limitation with this MEM-PTT model is that, as a consequence of assuming a single rate of breaking,  $\gamma$ , per puller position, vt i.e. E = E(vt), there must be a single position of the mass, X, for every position of the puller/sample, vt. If the rate of breaking is a one-to-one function of the puller position, the actual position of the mass does not matter. In reality, noise in the system will induce Brownian motion and the position of the mass can only be described statistically, i.e. with a probability distribution. The second limitation with MEM-PTT is one that has already been mentioned: it neglects damping of any form; in the PTT model,  $\eta_{\text{cantilever}} = \eta_{\text{bond}} = 0$ . Without damping, a real system would continue to move indefinitely, but real physical systems eventually lose energy to external systems. Both limitations—the lack of influence of the position X of the mass and the lack of damping—can be addressed by the Fokker–Planck (FP) equation [28].

The FP equation is a model from statistical mechanics which describes the probability distribution of a Brownian particle's position in a force field with damping. Brownian motion, the seemingly chaotic but stochastic diffusion of a particle under the influence of a potential energy landscape, arises from noise applied to the particle by internal (thermal) or external (mechanical) sources.

The FP equation is:

$$\frac{\partial P(X,t|X_0,t_0)}{\partial t} = \nabla \cdot \left(\nabla D - \frac{F(X,vt)}{\beta}\right) P(X,t|X_0,t_0),\tag{3.3}$$

where  $\beta$  is a general damping term, D is the diffusion coefficient which is a function of the noise characteristics, F(X, vt) is the position and time-dependent force field the mass experiences, and  $X_0$  is the initial position of the mass at the initial time  $t_0$ . This equation describes the probability distribution,  $P(X, t \mid X_0, t_0)$ , of the mass at position X at time t, given the initial position  $X_0$  at initial time  $t_0$ . Further manipulation of equation (3.3) provides a differential equation for the number of samples that remain, at time t:

$$\frac{\partial N(t|X_0, t_0)}{\partial t} = \int_{X=vt-X_c}^{X=vt+X_c} \nabla \cdot \left(\nabla D - \frac{F(X, vt)}{\beta}\right) P(X, t \mid X_0, t_0) N_0 dX, \tag{3.4}$$

where the limits correspond to the mass position X when the critical stretch length  $X_c$  is reached, in either direction. Using the divergence theorem, this becomes:

$$\frac{\partial N(t|X_0, t_0)}{\partial t} = \left(\nabla D - \frac{F(X, vt)}{\beta}\right) N(X, t \mid X_0, t_0) \bigg|_{X=vt - X_c}^{X=vt + X_c}$$
(3.5)

Comparing equations (3.2) and (3.5), both aim to describe the number of bonds that remain at time t, but their forms are clearly different.

Furthermore, distinguishing the probabilities from each analysis as  $P_{\text{FP}}$  and  $P_{\text{MEM}}$  for the FP and MEM respectively, the resulting analytical expressions for the average friction  $F_f$  can be compared:

$$\left\langle F_f^{FP} \right\rangle = \frac{1}{t} \int_0^t \int_{X=v\tau - X_c}^{X=v\tau + X_c} k_{\text{cant}} X P_{FP}(X, \tau \mid X_0, \tau_0) dX d\tau, \tag{3.6}$$

for the FP analysis and

$$\langle F_f^{\text{MEM}} \rangle = \frac{1}{t} \int_0^t k_{\text{cant}} f(v\tau) P_{\text{MEM}}(v\tau) d\tau,$$
 (3.7)

for the MEM. Here the mass position function  $f(v\tau)$  is intentionally left unspecified. In previously published MEM-PTT literature, this term is either set equal to the sample position x [7,14], or is approximated as a linear function of x [26]. Both forms are imprecise since the mass position X is required to calculate the instantaneous or average friction.

Another limitation with the MEM-PTT approach comes from the use of Kramer's rate. Briefly, the Kramer's rate models the transition rate of particles in a local energy minimum to an adjacent energy minimum when there is a local energy maximum in between the minima. The variable  $\gamma$  in equation (3.2) has been specified as the Kramer's rate in all past PTT literature that uses the MEM. However, the assumptions involved in deriving the Kramer's rate are violated in the frictional system described. Specifically, the Kramer's rate is derived assuming that the interaction is far from the local maximum of the potential (which must also be periodic because the Kramer's rate does not directly apply to an aperiodic harmonic tip-sample interaction potential) such that there is negligible diffusion past the barrier [27,29]. This assumption is violated in the PTT model where diffusion indeed takes place when the energy barrier has been significantly reduced by strain. The Kramer's rate derivation also assumes that the potential is time-independent, an underlying assumption of the PTT model. However, this is never true in a kinetic friction experiment which has a constantly time-evolving potential and a complete analysis should not impose this limiting condition.

A final concern that arises when using the Kramer's rate in juxtaposition with the MEM is how to interpret  $f_0$ , the attempt frequency. More than one issue surrounding  $f_0$  arises and, as is discussed in the SI,  $f_0$  is not well defined when using the MEM. However, for the discussion in this section, it will be assumed as in previous literature that  $f_0$  describes the frequency of the noise imposed on the mass, for the sake of making the clearest argument.

In such a case where  $f_0$  is the vibration frequency, as the puller stretches the bond and the cantilever, it becomes more likely that the bond will vibrate to an amplitude large enough to reach its critical stretch length and break. If the vibration frequency is high regardless of the stretch length, and assuming the tails of the stretch-length probability distribution do not go to zero before the critical stretch length (mathematically:  $\int_{v\tau-X_c}^{v\tau+X_c} P(X)dX > 0 \forall t, v$ ), then even with a small noise amplitude envelope the bond will break at small puller positions because the high noise frequency means the low-probability/high-amplitude stretch-length fluctuations happen frequently. Since the stick portion of stick-slip friction is readily observable in experiments, this very-early breaking is not experimentally justified. This widespread experimental observation indicates strongly that the stretch length can easily be relatively large before the percentage of bonds that break in a time  $\Delta t$  is significant. Yet at the typical experimental speeds of nanometers per second to tens of micrometers per second, once the stretch length reaches this regime, the vibration frequencies from atomic thermal movement are still so fast that the puller will have very little time to stretch the bond further before breaking occurs. If these points are valid, then two possible explanations are that the relevant vibration frequencies are significantly lower than atomic thermal vibration frequencies or that the common interpretation of the attempt frequency as an actual frequency is not accurate. Indeed, we will show for FP that friction will increase with increasing speed without requiring a single or narrow range of frequencies of the applied noise which have significantly higher amplitude in a power spectrum.

Regarding the former possibility—that the relevant vibration frequencies are significantly lower than atomic thermal vibration frequencies—if the attempt (vibration) frequency is much smaller (kilohertz or megahertz, instead of the terahertz for atomic thermal vibrations), the cantilever and bond springs can stretch by a significant amount before a breaking attempt is made. The smaller frequency spreads these additional vibrational stretches out in time so the dependence of the resulting measured friction force on them is clear. Indeed, several authors have previously discussed the fact that atomic vibration frequencies are likely not the source of thermal activation in friction experiments [14,16,21,30]. A recent result, along with showing the general inability of PTT to explain friction trends with temperature and speed, found that even the best fits to PTT required  $f_0$  values ranging from kHz to GHz [31]. Sang *et al.* treated  $\gamma$  as Kramer's rate, as they assumed the noise originated from mechanical resonances of the AFM. Riedo *et al.* [13] found that the attempt frequencies obtained from a fit to their friction-speed data put the attempt frequency in the kilohertz range. Additionally, Dong *et al.* explored the effect of kilohertz

royalsocietypublishing.org/journal/rsta Phil. Trans. R. Soc. A 380: 20210342

frequencies on friction using the MEM in a simulation setting [30]. However, because all these studies use the MEM-PTT model and because of the issues with the MEM discussed previously, the limitations of these interpretations should be considered.

#### 4. The MB model

The MB model was developed more recently to describe the non-monotonic dependence of friction on temperature seen in several studies, particularly at low temperatures, including groundbreaking work by Filippov, Schirmeisen *et al.*, Barel *et al.* and others [7,9–11,19]. Previously, these observations could not be explained by the PTT or any other model. These interesting results were very well fit by the MB model instead. The key physical insight was that the non-monotonicity of friction with temperature is a result of incorporating a rate of *formation* of interfacial bonds. This is accomplished by allowing the existence of some amount of time spent unbonded after the bond-breaking event has occurred, in contrast to the PTT model in which the bond always exists (since when it breaks, it immediately rebonds in a new position). Since in the MB model the rate of forming the bond increases with temperature, the time spent bonded increases and thus friction increases with temperature, up until a critical temperature at which the bond essentially forms instantly after a slip. In the case of a single MB bond site, the PTT behaviour is recovered above this critical temperature and friction accordingly decreases with further temperature increases due to thermally excited bond breaking.

The MB model is also distinct from the PTT model in allowing for as many bonds as desired, and as such it may more closely resemble the interface in an AFM contact experiment in that there are multiple interacting atoms or 'sites' in a contact which may have a heterogeneous character. The MB model can thus explore more complex collective behaviour (such as uncorrelated stickslip) than the more-specific PTT model. Analytical expressions are available for friction-speed and friction-temperature dependencies in the different friction-temperature regimes; furthermore, the full potential of the MB model is realized through the numerical *MB simulation algorithm* disseminated by Barel & Urbakh [9,11,19].

Very briefly, the MB algorithm solves  $F = m\ddot{X}$  for one or more linear-elastic bonds. If a site has not formed a bond, the time it has spent unbonded is compared to a random number chosen from an exponential distribution where the mean is the temperature-dependent rate of bonding and, if the time spent unbonded is greater than this random number, the bond forms. The bond is subsequently governed by the force equation until it is broken. The random number is sampled at every time step. Experimental results have been compared to such simulations and have shown consistent trends [9–11,19].

The MB model has some limitations to consider. In particular, a problem arises when determining the bond-breaking condition. The algorithm compares a temperature and stretch-length dependent number (which is proposed as an Arrhenius debonding rate) to a random number between zero and one taken from a uniform distribution; this is a Monte Carlo approach. The Monte Carlo approach is meant to simulate the effect of noise but creates the unphysical situation of the bond breaking before a critical stretch length,  $X_c$ . While a bond will stretch and contract in response to noise, it will not break until it is stretched by that critical amount. Note that, in comparison, a critical stretch length is implied by MEM-PTT.

One practical motivation for adopting the MB algorithm's Monte Carlo approach is related to the relevant vibration frequencies in nanoscale friction. If the bonds are vibrating at atomic thermal frequencies (ca 10<sup>13</sup> Hz), capturing the detailed dynamics of the system would require powerful processors, unphysically fast sliding speeds, and experimentally irrelevant short time durations to simulate any number of bonds. As mentioned in the section on the PTT model, another option exists: the applied noise can be given a flat frequency power spectrum, such as with white noise. Thus all arguments about an attempt frequency are avoided. This is the approach we take with the mMB algorithm. Another benefit of this approach, called the Weiner process, is that, though it is true that the range of applied frequencies depends on the time step and total time, the results do not.

royalsocietypublishing.org/journal/rsta Phil. Trans. R. Soc. A **380**: 20210342

## 5. The mMB model for the harmonic interaction potential with N=1: results and discussion

In order to demonstrate the ability of the mMB model and its algorithm to produce reasonable and experimentally supported friction results supported by the Fokker–Planck formalism, a MATLAB (Mathworks, Natick, Massachusetts) program based on the MB model and associated algorithm was developed with specific key modifications. As mentioned before, figure 1 illustrates the dynamic system that it simulates numerically for one bond but this can be expanded to an arbitrary number of bonds or modified to be a different interaction altogether, such as a periodic potential. The dynamic system with a harmonic interaction can be represented with the Langevin equation:

$$m\ddot{X} = \sum_{i=1}^{n} k_{\text{sub}}(x_i - X) - \eta_{\text{bond}}(\dot{X} - v) - k_{\text{cant}}X - \eta_{\text{cant}}\dot{X} + \zeta\sqrt{2\eta_{\text{cant}}k_{\text{B}}T}\epsilon_{\text{cant}} + \zeta\sqrt{2\eta_{\text{bond}}k_{\text{B}}T}\epsilon_{\text{sub}}$$
(5.1)

where  $k_B$  is Boltzmann's constant,  $\epsilon$  is a random Gaussian noise sample with mean  $\mu = 0$  and standard deviation  $\sigma = 1$ , n is the number of presently active bonds, and  $\zeta$  is the noise multiplier parameter which changes the average amplitude of the mechanical noise. For a single bond, i.e. n = 1, the dynamics are almost identical to those addressed by Reimann et al. [24,32], who was the first and so far only investigator to identify and explore the Fokker-Planck connection to nanoscale friction. By contrast with Reimann's work, in the mMB algorithm here, (1) the noise amplitude is not always set to that described by the fluctuation-dissipation theorem and is a tunable parameter  $\zeta$ , (2) there can be multiple bonds instead of one and (3) the bonds are linear springs whereas Reimann employed a sinusoidal potential in line with several PTT studies [6,12,14–17,24,26,30,32,33].

As mentioned, the Fokker-Planck equation describes the probability distribution of a particle's position while experiencing damping and other external environmental forces. As such, it provides a relevant description of the friction experienced by an AFM tip in a noisy environment and a good point of comparison of the accuracy of the mMB model. It is relevant when the force from damping is much greater than inertia, i.e.  $|\beta \dot{X}| \gg |m \dot{X}|$  (recall that  $\beta$  represents a general damping coefficient). For most cases involving AFM-based friction measurements, this is true due to the extremely small volumes of deformed material involved. Otherwise, the speed-dependence of friction would result from inertial effects, which by assumption is not the case.

For the case where n = 1, and  $|(\eta_{\text{sub}} + \eta_{\text{cant}})\dot{X}| \gg |m\ddot{X}|$ , equation (5.1) reduces to

$$(\eta_{\text{sub}} + \eta_{\text{cant}})\dot{X} = k_{\text{sub}}(vt - X) + \eta_{\text{sub}}v - k_{\text{cant}}X + \zeta \left(\sqrt{2\eta_{\text{sub}}k_{\text{B}}T} \times \epsilon_{\text{sub}} + \sqrt{2\eta_{\text{cant}}k_{\text{B}}T} \times \epsilon_{\text{cant}}\right),$$
(5.2)

and the Fokker-Planck equation representing the mMB simulations with these same conditions is

$$\frac{\partial P(X, t \mid X_0, t_0)}{\partial t} = \nabla \cdot \left( \nabla D - \frac{k_{\text{sub}}(vt - X) + \eta_{\text{bond}}v - k_{\text{cant}}X}{\eta_{\text{bond}} + \eta_{\text{cant}}} \right) P(X, t \mid X_0, t_0), \tag{5.3}$$

together with the moving boundary conditions  $P(X = vt - X_c, t) = P(X = vt + X_c, t) = 0$ . This boundary condition is a statement that the maximum length a bond can stretch in either direction before breaking (i.e. having a probability of zero) is the critical stretch length,  $X_{c.}$ 

The First-Slip Friction Force (FSFF), the quantity which will be of most interest when discussing results, is defined here as the friction force immediately before the bond (represented by the substrate spring) is broken, which occurs when it is stretched beyond length  $X_c$ . Figure 2 plots friction versus time simulated with the mMB algorithm. Figure 2 helps explain what the FSFF is and why it is the appropriate quantity to compare between mMB and FP results. In figure 2, the FSFF is indicated in the inset while the friction upon achieving dynamic equilibrium is bordered with a dashed box. The reason the FSFF is plotted as the main result in figure 3 instead of the more

royalsocietypublishing.org/journal/rsta

Phil. Trans. R. Soc. A 380: 20210342

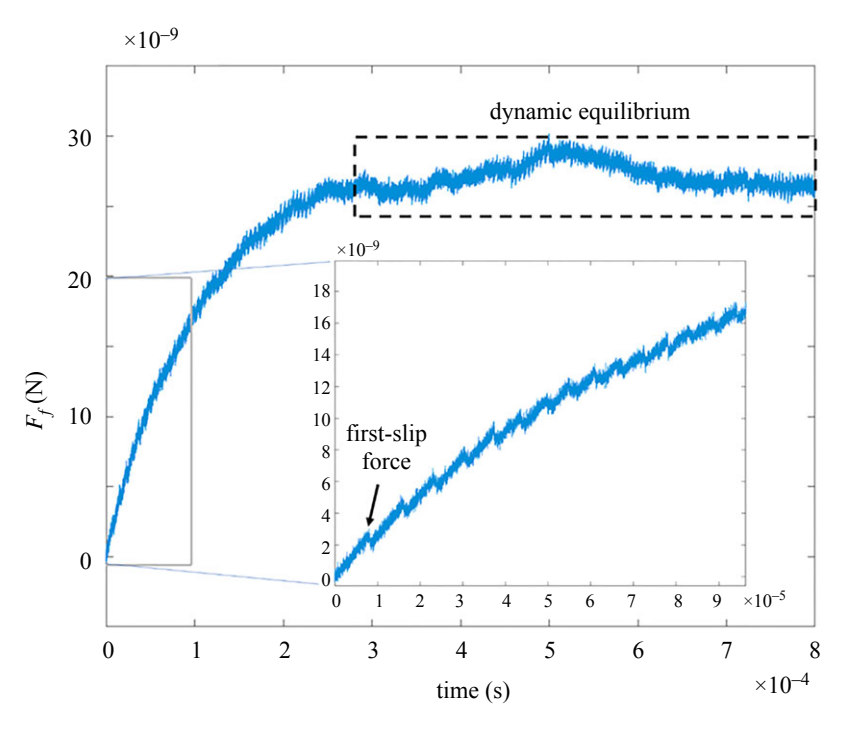


**Figure 2.** Illustration of the First-Slip Friction Force. This plots friction versus time for a system which does not reach dynamic equilibrium before or immediately after the first slip force. The solid-boxed region in the large plot is magnified (insert) showing the force upon the first slip (arrow). Notably, friction continues to evolve after the first slip; in this case the friction continues to increase while approaching the 'equilibrium' kinetic friction (dashed-boxed region), after which friction does not change in a time-averaged sense. (Online version in colour.)

commonly quoted time- and spatially averaged friction is that, when damping is present, after the first slip, highlighted in figure 2, the friction can continue to evolve to greater or lesser values after the first slip; represented by the 'dynamic equilibrium' region of figure 2. This is because the position of the mass, X, can continue to increase until a dynamic equilibrium is achieved wherein the forces on either side of the mass are balanced in a time-averaged sense. After the first slip, if the friction has not yet achieved dynamic equilibrium, the FP model is insufficient as it describes only one iteration of starting, pulling, and slipping, but before and during the first slip the FP model is valid. Notably, the MEM-PTT model is also incapable of describing such behaviour. While modifying the FP numerical simulations to account for further evolution after the first slip would be interesting and possible using more advanced statistical methods, the present work focuses solely on the region before and during the first slip of the mMB simulations.

It is interesting to note that the noise applied in the mMB and FP simulations is white noise which has a flat frequency spectrum. A clear increase of friction with speed is observed even without resorting to the idea of an attempt frequency which, as the interpretation commonly goes, has a single or narrow range of values, as we have previously discussed.

Figure 3 plots mMB and FP results for four values of  $\eta_{\rm cant}$ , with one plot per value, and several series within each plot using different noise multipliers  $\zeta$ —for mMB simulations—or diffusion coefficient D—for FP simulations. The value  $\eta_{\rm bond} = 6 \times 10^{-6} \, {\rm kg \, s^{-1}}$  was used in all plots and was chosen to be similar to the value used in [24,26] which was fit to data in [14,15]. The first observation from these plots we wish to highlight is the consistency in the results between the mMB and FP methods. To obtain similar maximum friction force versus v results in the FP results as the mMB simulations, the magnitudes of the noise multipliers  $\zeta$  (mMB) and the diffusion

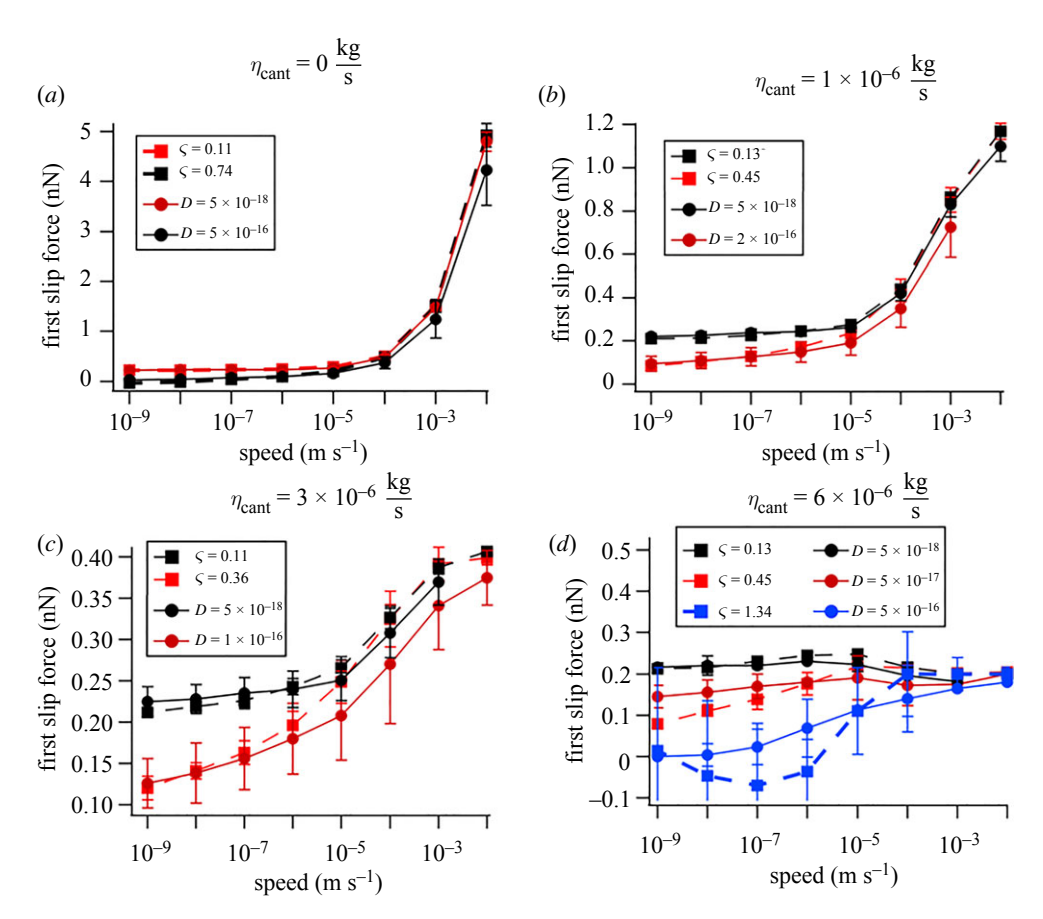


**Figure 3.** The First-Slip Friction Force versus speed for both Fokker–Planck (dashed lines) and modified multibond simulations (solid lines), with particular noise multipliers ( $\zeta$ ) and diffusion coefficients (D) as indicated in the legends. The cantilever damping coefficient used in each series is shown above its respective plot. The parameters common to each series are  $\eta_{\text{sub}} = 6 \times 10^{-6} \text{ kg s}^{-1}$ ,  $k_{\text{sub}} = 1.3 \text{ N m}^{-1}$ ,  $k_{\text{cant}} = 1.3 \text{ N m}^{-1}$ ,  $k_{\text{c}} = 2 \text{ Å}$ , and  $k_{\text{c}} = 1.3 \text{ N}$  (Online version in colour.)

coefficients D (FP) had to be changed in tandem. Therefore, the mMB algorithm, in its most basic form where N = 1, is validated by the fundamental foundation that is the FP equation.

In the discussion so far we have explored limitations of existing models for nanoscale thermally influenced friction, provided an alternative (the mMB model), and shown the validity of the alternative. We emphasize that the results of figure 3 do not necessarily represent what may happen in a true experiment; after all, very few systems can accurately be represented by a single bond. Because of this it should not be concerning that there is no levelling off or downturn of friction at speeds of approximately  $10\,\mu\text{m s}^{-1}$  as is frequently observed in experiments. In the next section, we will apply the mMB algorithm—using multiple bonds as well as a periodic potential—in a study of the origins of the levelling off or downturn. These simulations will be more relevant to experiments.

# 6. The mMB model for the harmonic interaction potential with N > 1 and for the periodic interaction potential

A full-factorial design of experiment (DOE) was run using the mMB and FP algorithms with a periodic potential for the surface-tip interaction. The three factors were (1)  $\eta_S$  with the three levels of 0,  $1 \times 10^{-6}$ , and  $6 \times 10^{-6}$  kg s<sup>-1</sup>, (2)  $\eta_C$  with the two levels of  $1 \times 10^{-6}$ , and  $6 \times 10^{-6}$  kg s<sup>-1</sup>, and

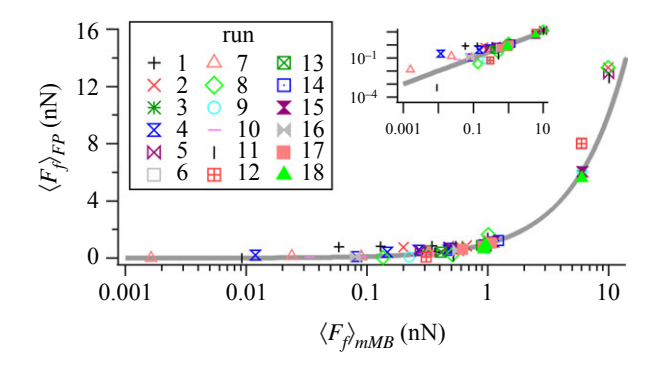


**Figure 4.** The average friction from FP simulations versus the average friction from mMB simulations using a periodic potential for the surface-tip interaction (bond). The gray curve represents a perfect match. (Online version in colour.)

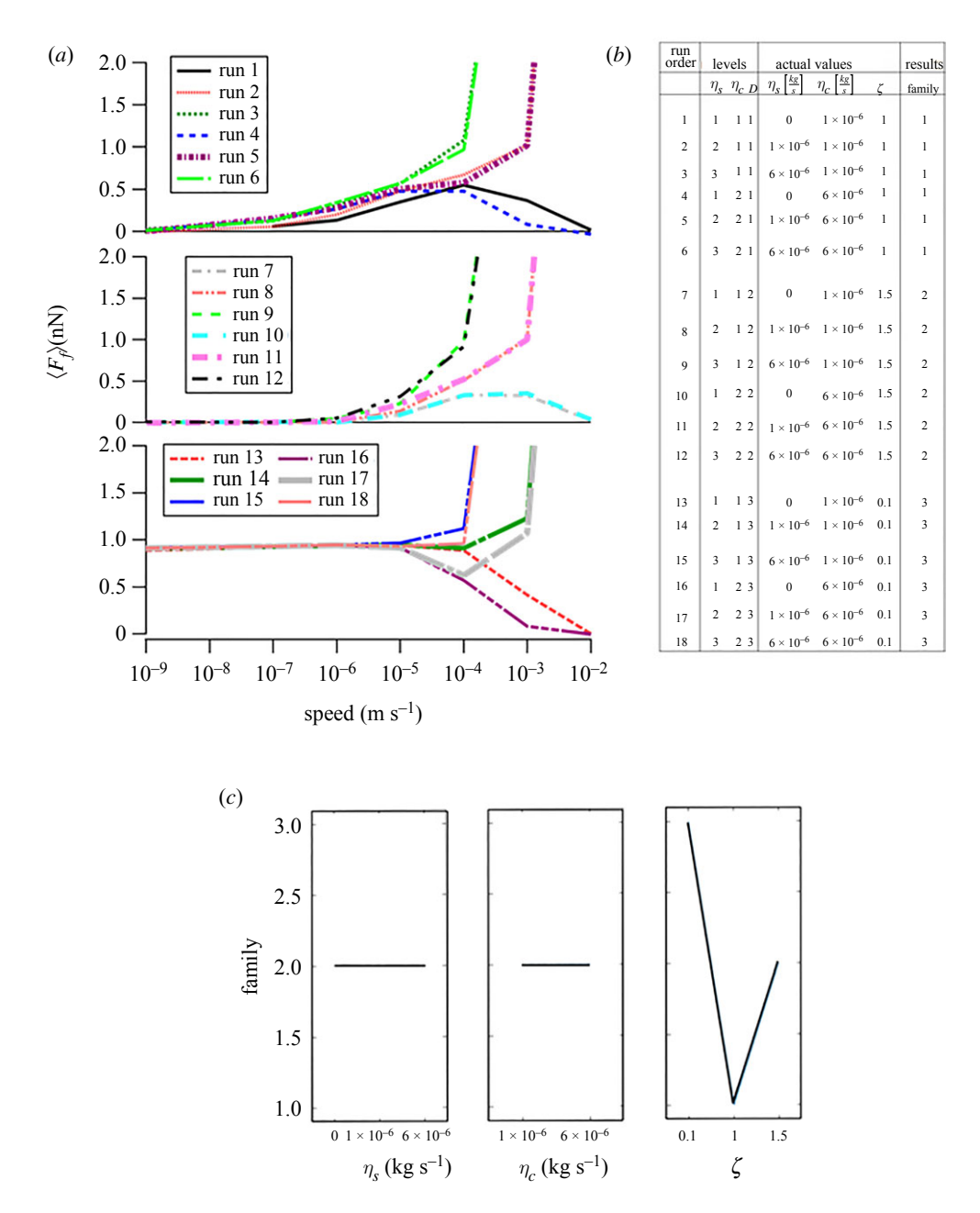
(3)  $\zeta$  with the three levels of 0.1, 1.0, and 1.5. This design required 18 total simulations for each algorithm. The cantilever spring constant,  $k_c$ , was held constant at  $1.0\,\mathrm{N\,m^{-1}}$ . Figure 4 plots the average friction from the FP algorithm for all runs,  $\langle F_f \rangle_{FP}$ , against the average friction from the mMB algorithm for all runs,  $\langle F_f \rangle_{mMB}$ , clearly showing that they match very closely. This is another demonstration of the validity of the mMB algorithm.

Figure 5a shows the average friction from this DOE for the mMB algorithm plotted against speed in three plots. Three plots are shown because the curves ended up grouping into three families, comprising similar trends, which we arbitrarily label families 1, 2 and 3. Figure 5b is a legend for each curve which also expresses to which family the curve belongs. Figure 5c plots the main effect of family grouping for each factor. Clearly, the only influence on family is the noise factor, c.

Before turning to results from the design of experiment for the mMB algorithm using the harmonic potential, we note that (1) the periodic potential shows a clear downturn in the average friction at fast speeds in some cases, and (2) we were able to reproduce the results of Reimann [24] and share those in electronic supplementary material, figure S1.

In order to compare average friction results using different tip-surface potentials and with more experimentally realistic conditions, a full-factorial design of experiment was also run using the harmonic (spring) potential for the surface-tip interaction. The three factors were (1)  $\eta_{\rm S}$  with two levels of  $3\times10^{-6}$ , and  $6\times10^{-6}\,{\rm kg\,s^{-1}}$ , (2)  $\zeta$  with the three levels of 0.022, 11.192 and 22.361 (these specific, precise numbers were chosen simply because they were found to enable convenient calculations in our numerical algorithm) and (3) N, the number of tip-surface interactions using the harmonic potential, with two levels of 5 and 40. This resulted in 12 total runs. The cantilever damping constant, substrate spring constant and cantilever spring constant ( $\eta_{\rm C}$ ,  $k_{\rm S}$  and  $k_{\rm C}$ , respectively) were held constant at  $6\times10^{-6}\,{\rm kg\,s^{-1}}$ ,  $20\,{\rm N\,m^{-1}}$  and  $10\,{\rm N\,m^{-1}}$ , respectively. The mMB algorithm was used since the FP algorithm, in its current state, does not incorporate more than one tip-surface interaction.

Prior to running this design, a fractional factorial design was run with the base mMB algorithm, but friction did not change significantly with changing speed for all but one run. These results are in the supporting information. A probable reason for this behaviour is that, with the base algorithm and simulating multiple bonds, the fact that bonds can form regardless of location with respect to the substrate causes bonds to be stretched in random amounts at any given time. Single bond-breaking events do not lead to a significant change in mass position and velocity as the mass recoils from the single broken bond since there are plenty of only mildly stretched bonds to absorb the impact. This leads to a relatively smooth friction trace, similar to traces on amorphous surfaces. We hypothesize then that the velocity dependence of friction is strongest when bonds are broken in concert, leading to obvious stick-slip behaviour. Therefore, the algorithm was changed to only form a bond when the tip was within a predetermined distance



**Figure 5.** Results from the full-factorial design of experiment from mMB algorithm simulations using the periodic potential for the tip-surface interaction. (a)  $\langle F_f \rangle$  versus *Speed* for all 18 runs, separated into three families. (b) Legend and family for each curve. (c) main effects of each factor. (Online version in colour.)

 $d_0$  from sites spaced evenly apart in the sliding direction. We set  $d_0 = 2$  Å. Note that N bonds with  $k_{\mathrm{sub}-N}$ , acting in perfect concert (i.e.  $d_0 = 0$ ), is identical to one bond with  $k_{\mathrm{sub}-1} = N * k_{\mathrm{sub}-N}$ . In other words, the results for N = 1 shown previously are the limiting case of  $d_0 = 0$ .

We call this scheme the *correlated* stick-slip algorithm and the base algorithm the *uncorrelated* algorithm or just 'the mMB algorithm'. The Correlated mMB algorithm was used to run the full-factorial design described in the previous paragraph.

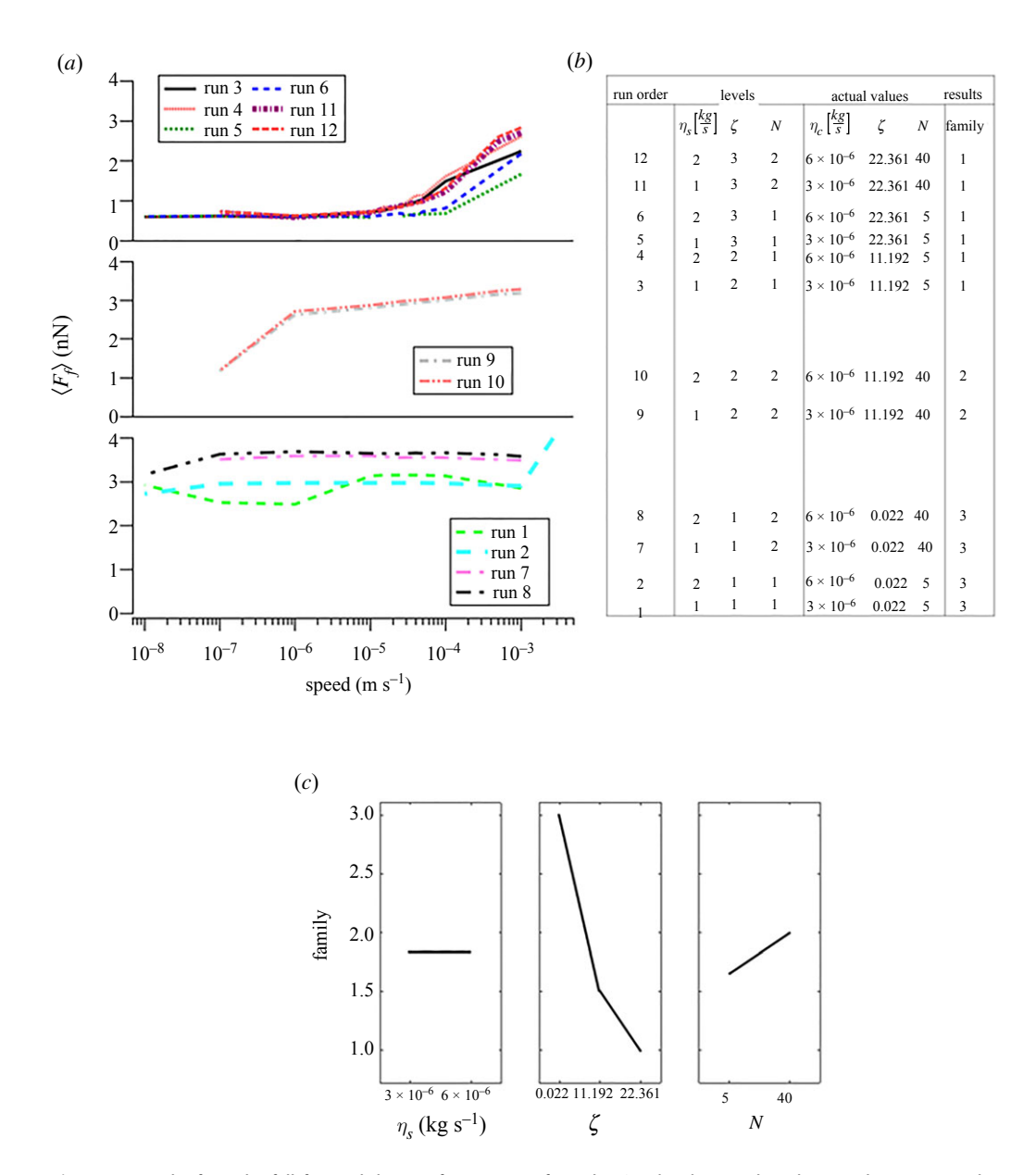


**Figure 6.** Results from the full-factorial design of experiment from the *Correlated* mMB algorithm simulations using the harmonic potential for the tip-surface interaction. (a)  $\langle F_f \rangle$  versus *Speed* for all 12 runs, separated into three families. (b) Legend and family for each curve. (c) main effects of each factor. (Online version in colour.)

Figure 6a shows the average friction from this design for the Correlated mMB algorithm plotted against speed in three plots. As in the case for the periodic potential results, three plots are shown because the curves grouped into three *families*, which we again arbitrarily label families 1, 2 and 3. Figure 6b is a legend for each curve which also expresses to which family the curve belongs. Figure 6c plots the main effect of family grouping for each factor. Similar to the periodic potential results, the noise,  $\zeta$ , plays the most significant role in family determination. The number of sites, N, plays a minor but certain role in family determination. As with the periodic potential, the substrate damping coefficient,  $\eta_S$ , plays no role in family determination.

It is notable that family 2 is the only one which resembles the logarithmic increase followed by levelling at higher speeds of the PTT theory and constituent experimental results. Also, no combination of factors tested here resulted in a clear decrease of average friction with increasing speed as was seen in the periodic potential results. Though we have tested other aspects such as setting the lower level of  $\eta_S$  equal to zero, changing the spring constants  $k_S$  and  $k_C$ , and increasing the noise level  $\zeta$ —rerunning the design with every incremental change—the average friction versus speed trend never decreases systematically at fast speeds. However, in many cases, the average friction does level off at fast speeds, as seen experimentally. These observations deepen the mystery as to which potential, when used in the mMB algorithm, better represents experiments: periodic or harmonic with many interactions. Testing friction at faster speeds than shown experimentally so far will help to shed light on this mystery.

#### 7. Conclusion

In this study, assumptions, advantages, and limitations of the most commonly used models for nanoscale friction—the PTT model and the multibond numerical method—were discussed. We identified some unphysical assumptions; particularly, the Master Equation method and the use of Kramer's rate in the PTT model and the Monte Carlo approach to bond-breaking in the MB model. A new model, the modified multibond model (mMB), is presented. It includes the independent effects of damping and noise on the cantilever and the sample and enforces a critical stretch length criterion for bond-breaking. The modified multibond results agree well with numerical Fokker–Plank simulations of friction in a harmonic potential, the latter being a rigorously derived statistical mechanics relation. The mMB model can be further modified to explore much more complex systems, including those with multiple bonding sites, correlated stick slip, and uncorrelated stick slip. It can replicate the experimental results of friction increasing approximately with the logarithm of the scanning speed, and may help elucidate whether and when friction plateaus or decreases at faster speeds, sliding speeds that have yet to be explored experimentally.

Data accessibility. Codes for the mMB and FP numerical algorithms can be found on GitHub.com [34,35]. All simulation data are available upon request. The data are provided in electronic supplementary material [36]. Authors' contributions. Z.M.: conceptualization, formal analysis, investigation, methodology, writing—original draft, writing—review and editing; K.H.: methodology, writing—review and editing; JB.M.: methodology, writing—review and editing; J.C.: formal analysis, software; R.C.: conceptualization, funding acquisition, investigation, project administration, supervision, writing—original draft, writing—review and editing.

All authors gave final approval for publication and agreed to be held accountable for the work performed therein.

Conflict of interest declaration. We declare we have no competing interests.

Funding. This work was supported by the Air Force Office of Scientific Research under grant no. FA2386-18-1-4083, and by the US National Science Foundation under awards CMMI-1761874 and the University of Pennsylvania Materials Research Science and Engineering Center grant no. NSF-DMR-1720530. Z.M. acknowledges support from the National Science Foundation under Veterans Research Supplement CMMI-1640271. K.H. acknowledges support from the National Science Foundation Graduate Research Fellowship under grant no. DGE-1845298.

Acknowledgements. We acknowledge Z. Brannigan and K. Kroker for enlightening discussions and M. Urbakh who helped clarify aspects of the multibond model.

## Appendix A. Methodology

In the mMB simulation algorithm the fourth-order Runge–Kutta method was used. At each time step, displacement equivalent to

$$\zeta \Gamma \left( \mu = 0, \sigma = \sqrt{\frac{2\eta_{\text{bond}}k_{\text{B}}T}{\Delta t}} \right) + \zeta \Gamma \left( \mu = 0, \sigma = \sqrt{\frac{2\eta_{\text{cant}}k_{\text{B}}T}{\Delta t}} \right)$$
 (A.1)

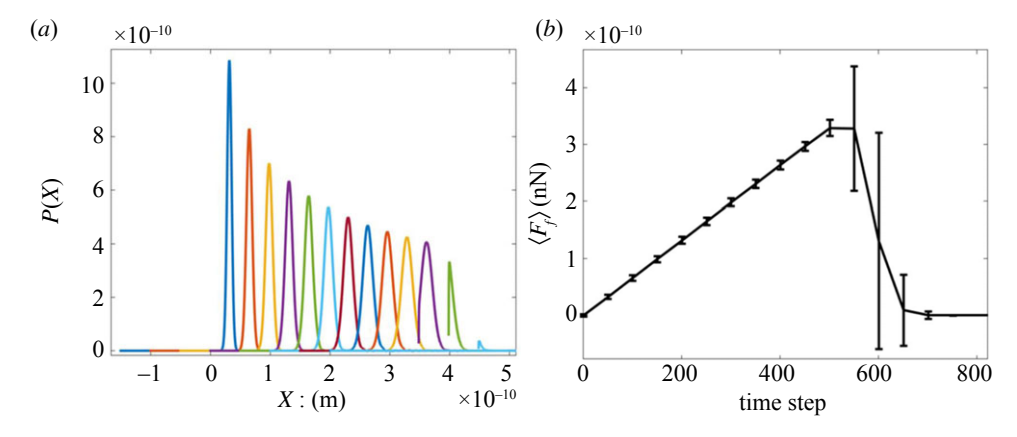


**Figure 7.** (a) Mass position probability distributions at different times. (b) Corresponding average friction force. $v=1~\mu$  m s<sup>-1</sup>,  $D=1\times10^{-16}$ ,  $k_s=1.3~N~m^{-1}$ ,  $k_c=1~N~m^{-1}$ ,  $\eta_{cant}=3\times10^{-6}$  kg s<sup>-1</sup>,  $\eta_{bond}=6\times10^{-6}$ kg s<sup>-1</sup>,  $\chi_{c}=2~\text{Å}$ , and T=300~K. (Online version in colour.)

is added to the system following equation (5.1). This is the source of noise. The time step,  $\Delta t$ , showing up in the denominator of the square root in the standard deviation, is a characteristic of the *discrete* Wiener Process. Without this term, the results would differ for different time steps.

The Wiener process dictates that the noise be white noise and, as such, the power spectral density is flat across all frequencies. This fact means that, in the mMB framework, any particular frequency of the noise cannot be taken as an independent contributor to any phenomenon, as is often suggested when alluding to the idea of an 'attempt frequency'.

Here,  $\Gamma$  is a normal distribution with mean  $\mu$  and standard deviation  $\sigma$ . The procedure for determining when a bond is formed is identical to the original MB algorithm. A bond-forming activation energy of  $1.5 \times 10^{-20} \text{J}$  is used to match the previous work [9–11,19] and can be tuned as needed. However, for comparison with the FP theoretical framework proposed in this article (which may be modified to incorporate n > 1 as well as the effect of having a rate of forming the bond), there is no effect of forming a bond in the FP theoretical framework as it is only concerned with first slip and not with what happens after the bond is broken. The breaking condition occurs when the bond reaches the critical stretch length  $X_c$ , which is set to 2 Å. This critical stretch length can be tuned for different materials and interactions. To compare the FP equation to the mMB results, equation (5.3) was solved using COMSOL's (Burlington, MA) partial-differential equation solver. The initial normal distribution of mass positions  $P(X,0 \mid 0.0)$  is given a standard deviation of 0.01 Å to approximate a delta function. The set-up utilizes a moving mesh domain X of  $vt-X_c \leq X \leq vt+X_c$  where the boundary conditions are  $P(X=vt-X_c,t)=P(X=vt+X_c,t)=0$ . The raw P(X,t) results are exported to MATLAB where the numerical integrations to obtain the mean and standard deviation of  $F_f$  at each time step are performed.

Figure 7 shows several snapshots in time of the Fokker–Planck COMSOL simulation. Figure 7a shows the probability P(X) of the particle (mass) being at a given position X, while figure 7b shows the mean friction force  $F_f$  versus puller position x at the same instances in time. As the puller moves forward the distance between the puller and mass increases and thus, so does the friction. The total probability  $\int_X P(X) dX$  decreases as interactions break once they reach the critical stretch length  $X_c$ . At a certain point all interactions have reached a stretch length of  $X_c$  and the friction rapidly drops to zero. Note that the time steps in simulations are much finer than shown in figure 7, which selects a sample of time steps for clarity.

#### References

1. Carpick RW, Salmeron M. 1997 Scratching the surface: fundamental investigations of tribology with atomic force microscopy. *Chem. Rev.* **97**, 1163–1194. (doi:10.1021/cr960068q)

- Szlufarska I, Chandross M, Carpick RW. 2008 Recent advances in single-asperity nanotribology. J. Phys. D. Appl. Phys. 41, 123001. (doi:10.1088/0022-3727/41/12/123001)
- 3. Homola AM, Israelachvili JN, Mcguiggan PM, Gee ML. 1990 Fundamental experimental studies in tribology: the transition from 'interfacial' friction of undamaged molecularly smooth surfaces to 'normal' friction with wear. *Wear* **136**, 65–83. (doi:10.1016/0043-1648(90)90072-I)
- 4. Prandtl L. 1928 A conceptual model to the kinetic theory of solid bodies. *Zeitschrift für Angew*. **8**, 85–106. (doi:10.1002/zamm.19280080202)
- 5. Tomlinson GA. 1929 A molecular theory of friction. *London, Edinburgh, Dublin Philos. Mag. J. Sci.* 17, 147–156.
- Gnecco E, Roth R, Baratoff A. 2012 Analytical expressions for the kinetic friction in the Prandtl-Tomlinson Model. *Phys. Rev. B - Condens. Matter Mater. Phys.* 86, 1–6. (doi:10.1103/ PhysRevB.86.035443)
- 7. Filippov AE, Klafter J, Urbakh M. 2004 Friction through dynamical formation and rupture of molecular bonds. *Phys. Rev. Lett.* **92**, 135503. (doi:10.1103/PhysRevLett.92.135503)
- 8. Gnecco E, Bennewitz R, Gyalog T, Meyer E. 2001 Friction Experiments on the Nanometre Scale. *J. Phys.: Condens. Matter* 13, R619–R642. (doi:10.1088/0953-8984/13/31/202)
- 9. Barel I, Urbakh M, Jansen L, Schirmeisen A. 2010 Multibond dynamics of nanoscale friction: the role of temperature. *Phys. Rev. Lett.* **104**, 1–4. (doi:10.1103/PhysRevLett.104.066104)
- 10. Schirmeisen A, Jansen L, Hölscher H, Fuchs H. 2006 Temperature dependence of point contact friction on silicon. *Appl. Phys. Lett.* **88**, 123108. (doi:10.1063/1.2187575)
- 11. Barel I, Urbakh M, Jansen L, Schirmeisen A. 2011 Unexpected temperature and velocity dependencies of atomic-scale stick-slip friction. *Phys. Rev. B Condens. Matter Mater. Phys.* 84, 1–7. (doi:10.1103/PhysRevB.84.115417)
- 12. Gnecco E, Riedo E, Bennewitz R. 2003 Thermally activated phenomena observed by atomic force microscopy. *MRS Online Proceedings Library* **790**, 13. (doi:10.1557/PROC-790-P1.3)
- 13. Bennewitz R, Gnecco E, Gyalog T, Meyer E. 2001 Atomic friction studies on well-defined surfaces. *Tribol. Lett.* **10**, 51–56. (doi:10.1023/A:1009078329570)

Downloaded from https://royalsocietypublishing.org/ on 09 August 2022

- 14. Riedo E, Gnecco E, Bennewitz R, Meyer E, Brune H. 2003 Interaction potential and hopping dynamics governing sliding friction. *Phys. Rev. Lett.* **91**, 084502. (doi:10.1103/PhysRevLett.91.084502)
- 15. Gnecco E, Bennewitz R, Gyalog T, Loppacher C, Bammerlin M, Meyer E, Güntherodt H-J. 2000 Velocity dependence of atomic friction. *Phys. Rev. Lett.* **84**, 1172–1175. (doi:10.1103/PhysRevLett.84.1172)
- 16. Liu X-Z, Ye Z, Dong Y, Egberts P, Carpick RW, Martini A. 2015 Dynamics of atomic stick-slip friction examined with atomic force microscopy and atomistic simulations at overlapping speeds. *Phys. Rev. Lett.* **114**, 1–5. (doi:10.1103/PhysRevLett.114.146102)
- 17. Li Q, Dong Y, Perez D, Martini A, Carpick RW. 2011 Speed dependence of atomic stick-slip friction in optimally matched experiments and molecular dynamics simulations. *Phys. Rev. Lett.* **106**, 126101. (doi:10.1103/PhysRevLett.106.126101)
- 18. Jansen L, Hölscher H, Fuchs H, Schirmeisen A. 2010 Temperature dependence of atomic-scale stick-slip friction. *Phys. Rev. Lett.* **104**, 1–4. (doi:10.1103/PhysRevLett.104.256101)
- 19. Barel I, Urbakh M, Jansen L, Schirmeisen A. 2010 Temperature dependence of friction at the nanoscale: when the unexpected turns normal. *Tribol. Lett.* **39**, 311–319. (doi:10.1007/s11249-010-9675-4)
- 20. Zhao X, Hamilton M, Sawyer WG, Perry SS. 2007 Thermally activated friction. *Tribol. Lett.* 27, 113–117. (doi:10.1007/s11249-007-9220-2)
- 21. Krylov SY, Jinesh KB, Valk H, Dienwiebel M, Frenken JWM. 2005 Thermally induced suppression of friction at the atomic scale. *Phys. Rev. E Stat. Nonlinear, Soft Matter Phys.* **71**, 1–4. (doi:10.1103/PhysRevE.71.065101)
- Carpick RW, Ogletree DF, Salmeron M. 1997 Lateral stiffnessâÁr: a new nanomechanical measurement for the determination of shear strengths with friction force microscopy. *Appl. Phys. Lett.* 70, 1548. (doi:10.1063/1.118639)
- 23. Lantz MA, O'Shea SJ. 1997 Lateral stiffness of the tip and tip-sample contact in frictional force microscopy. *Appl. Phys. Lett.* **70**, 970. (doi:10.1063/1.118476)
- Reimann P, Evstigneev M. 2004 Nonmonotonic velocity dependence of atomic friction. *Phys. Rev. Lett.* 93, 230802. (doi:10.1103/PhysRevLett.93.230802)

royalsocietypublishing.org/journal/rsta

- 25. Shao Y, Jacobs TDB, Jiang Y, Turner KT, Carpick RW, Falk ML. 2017 A multi-bond model of single-asperity tribochemical wear at the nano-scale. *ACS Appl. Mater. Interfaces* **9**, 35333–35340. (doi:10.1021/acsami.7b08023)
- 26. Sang Y, Dubé M, Grant M. 2001 Thermal effects on atomic friction. *Phys. Rev. Lett.* 87, 174301. (doi:10.1103/PhysRevLett.87.174301)
- 27. Kurkijarvi J. 1972 Intrinsic fluctuations in a superconducting ring closed with a josephson junction. *Phys. Rev. B* **6**, 832–835. (doi:10.1103/PhysRevB.6.832)
- 28. Risken H. 1984 *The fokker-Planck equation*. Berlin, Germany: Springer.
- 29. Chandrasekhar S. 1943 Stochastic Problems in Physics and Astronomy. *Rev. Mod. Phys.* **15**, 1–89. (doi:10.1103/RevModPhys.15.1)
- 30. Dong Y, Gao H, Martini A, Egberts P. 2014 Reinterpretation of Velocity-Dependent Atomic Friction: Influence of the Inherent Instrumental Noise in Friction Force Microscopes. *Phys. Rev. E Stat. Nonlinear, Soft Matter Phys.* **90**, 1–8. (doi:10.1103/PhysRevE.90.012125)
- 31. Hasz KR, Vazirisereshk MR, Martini A, Carpick RW. 2021 Bifurcation of nanoscale thermolubric friction behavior for sliding on MoS<sub>2</sub>. *Physical Review Materials* **5**, 083607. (doi:10.1103/PhysRevMaterials.5.083607)
- 32. Reimann P, Van den Broeck C, Linke H, Hänggi P, Rubi JM, Pérez-Madrid A. 2002 Diffusion in tilted periodic potentials: enhancement, universality, and scaling. *Phys. Rev. E Stat. Physics, Plasmas, Fluids, Relat. Interdiscip. Top.* **65**, 1–16. (doi:10.1103/PhysRevE.65.031104)
- 33. Müser MH. 2011 Velocity dependence of kinetic friction in the Prandtl-Tomlinson Model. *Phys. Rev. B Condens. Matter Mater. Phys.* **84**, 125419. (doi:10.1103/PhysRevB.84.125419)
- 34. Milne ZB. 2018 Modified Multibond Model Numerical Algorithm. See https://github.com/zmilne/Modified-Multibond-Model-numerical-simulations/tree/zmilne-patch-1
- 35. Milne ZB. 2018 Fokker-Planck Simulations. See https://github.com/zmilne/Modified-Multibond-Model-numerical-simulations/tree/master.
- 36. Milne ZB, Hasz K, McClimon JB, Castro J, Carpick RW. 2022 A modified multibond model for nanoscale static friction. Figshare. (doi:10.6084/m9.figshare.c.6026343)